



1 **Long-term multi-source precipitation estimation with high resolution**  
2 **(RainGRS Clim)**

3

4 **Anna Jurczyk<sup>1</sup>, Katarzyna Ośródka<sup>1</sup>, Jan Szturc<sup>1</sup>, Magdalena Pasierb<sup>1</sup>, and Agnieszka Kurcz<sup>1</sup>**

5

6 <sup>1</sup>Centre of Meteorological Modelling, Institute of Meteorology and Water Management – National Research  
7 Institute, ul. Podleśna 61, 01-673 Warsaw, Poland

8

9

10

11 **Correspondence:** Jan Szturc ([jan.szturc@imgw.pl](mailto:jan.szturc@imgw.pl))

12



13 **Abstract.** This paper explores the possibility of using multi-source precipitation estimates for  
14 climatological applications. A data processing algorithm (RainGRS Clim) has been developed to work  
15 on precipitation accumulations such as daily or monthly totals, which are significantly longer than  
16 operational accumulations (generally between 5 min and 1 h). The algorithm makes the most of  
17 additional opportunities, such as the possibility to complement with delayed data, access to high-quality  
18 data that are not operationally available, and the greater efficiency of the algorithms for data quality  
19 control and merging on longer accumulations. Verification of the developed algorithms was carried out  
20 on monthly accumulations through comparison with precipitation from manual rain gauges. As a result,  
21 monthly accumulations estimated by RainGRS Clim were found to be significantly more reliable than  
22 accumulations generated operationally. This improvement is particularly noticeable for the winter  
23 months, when precipitation estimation is much more difficult due to less reliable radar estimates.

24

## 25 1. Introduction

26

27 The estimation of precipitation on the ground surface with high spatial resolution is one of the  
28 most important issues in meteorology, but at the same time one of the most complex because of the very  
29 high spatial and temporal variability of precipitation, especially in the case of intense events associated  
30 with convective phenomena. This makes its precise quantitative estimation very difficult and subject to  
31 many errors. None of the available techniques, i.e. rain gauge measurements, meteorological radar  
32 measurements or satellite estimates based on measurements in different electromagnetic radiation bands,  
33 provide satisfactory precision. Consequently, different methods are being developed to combine  
34 precipitation data obtained by these techniques, with the aim of exploiting the advantages of each  
35 technique while minimising its weaknesses (Ochoa-Rodriguez et al., 2019; Jurczyk et al., 2020b;  
36 Wetchayont et al., 2023).

37 The generation of such multi-source precipitation estimates is currently the standard procedure  
38 used for quantitative precipitation estimation (QPE). In operational (i.e. real-time) applications, the most  
39 common time step for estimating the precipitation field is the 1-hour step, as it often follows the demand  
40 from hydrological rainfall-runoff models (Sokol et al., 2021). However, sub-hourly resolutions, such as  
41 10-minute resolution, are also increasingly used. Such data are becoming essential, in particular as input  
42 for nowcasting precipitation forecast models, for precipitation-runoff models forecasting flash floods,  
43 which are triggered by intense but short-lived and rapidly fluctuating precipitation (e.g., Chan et al.,  
44 2016; Neuper and Ehret, 2019), or for performing analyses of the occurrence of precipitation extremes  
45 (e.g., Bonaccorso et al., 2020; Lengfeld et al., 2020; Marra et al., 2022).

46 However, there is also growing demand among climatologists and agrometeorologists, for  
47 example, for longer precipitation totals – of the order of days, months or years, or even entire multi-year  
48 periods – that still maintain high spatial resolution. This demand can in fact already be met, as radar  
49 observations of precipitation, providing the highest spatial resolution of all measurement techniques,



50 have been performed routinely for several decades. So, long series of radar as well as multi-source  
51 precipitation estimates are already available. Weather radar networks have covered a large part of the  
52 more densely populated areas of the globe, so that increasingly radar data, when supplemented with  
53 other observations, are also applied in climatological studies to provide extensive information on the  
54 multi-year variability of the precipitation field with very high spatial resolution not available with other  
55 measurement techniques (Fabry et al., 2017; Saltikoff et al., 2019a). They are also used to study the  
56 climatology of intense convective phenomena, as the high spatial resolution is particularly important in  
57 this case (Hamidi et al., 2017; Burcea et al., 2019; Voormansik et al., 2021; Hänsler and Weiler, 2022;  
58 Piscitelli et al., 2022).

59 Consequently, there is a need to produce reliable estimates of precipitation accumulation over  
60 longer time periods (daily, monthly, yearly, or even longer) with data from databases containing  
61 operationally generated multi-source precipitation at higher temporal resolutions, e.g. as 10-min  
62 precipitation accumulations. It turns out that simply adding up, for example, 10-min estimates does not  
63 give satisfactory results, because any quality control algorithms for precipitation observations become  
64 much more effective for longer accumulations of at least 1 hour (Morbidei et al., 2018; Villalobos-  
65 Herrera et al., 2022). In particular, any algorithms for the adjustment of radar to rain gauge data often  
66 work too randomly when shorter accumulations are used, and the cross-checking of different types of  
67 precipitation data is then also subject to much higher uncertainty.

68 Generating accumulations for longer time intervals therefore provides the possibility of carrying  
69 out so-called reanalyses, i.e. re-generating the corresponding precipitation accumulation. This brings the  
70 following potential benefits: (i) data sets can be supplemented with data that were missing from the  
71 operational estimation, e.g. due to delays in their arrival at the system, (ii) in addition, data from such  
72 measurement techniques that are available too late for operational applications, or measured with a  
73 longer calculation step (e.g. daily, such as from manual rain gauges) can be used (Imhoff et al., 2021),  
74 (iii) algorithms for performing quality control on radar precipitation data and then combining them with  
75 data from other sources generally work much more effectively on longer accumulations (Wagner et al.,  
76 2012; Park et al., 2019).

77 Various initiatives are being undertaken to estimate precipitation data for climatological purposes  
78 with the high spatial resolution obtained from radar observations, including on a trans-national scale.  
79 One of the major initiatives in this area is the EURADCLIM (EUropean RADar CLIMatology) dataset,  
80 which is based on radar data obtained from the Operational Program on the Exchange of Weather Radar  
81 Information (OPERA) – a EUMETNET (EUropean METeorological NETwork) initiative (Saltikoff et  
82 al., 2019b), and rain gauge data obtained from the European Climate Assessment & Dataset (ECA&D)  
83 project. Both of these networks are pan-European and cover the area of most of Europe. In the  
84 EURADCLIM programme, radar quality control adapted to longer precipitation accumulation intervals,  
85 such as 1-h and daily intervals, is performed (Overeem et al., 2023). Quality control is also performed  
86 on longer rain gauge accumulations within ECA&D (Klok and Klein Tank, 2009).



87 The concept of generating long-term precipitation estimation presented in this paper is based on  
 88 using algorithms for quality control of the input data and combining them into multi-source estimates,  
 89 which are applied operationally to 10-min data. However, new quality control methods and new data  
 90 sources were also included – something that was not possible during the operational generation of  
 91 precipitation estimates.

92 Section 2 describes all input data, those available operationally as well as those used for  
 93 reanalyses. Section 3 presents the algorithm for combining precipitation data into a multi-source  
 94 precipitation field, used both operationally and for reanalyses, and Section 4 proposes a scheme for  
 95 generating long-term estimates. Section 5 shows and discusses the results of the verification of the  
 96 reanalyses of monthly totals in different seasons compared to operationally generated estimates, while  
 97 Section 6 shows an example of the system performance. Finally, Section 7 provides conclusions.

98

## 99 2. Precipitation data

100

### 101 2.1. Precipitation measurement data available for the area of Poland

102

103 Table 1 summarises the general characteristics of the precipitation data available for the area of  
 104 Poland: from in situ and remote sensing measurements, available both in real-time and after a shorter or  
 105 longer processing time, which can take up to two months (this is the case for quality control of the data  
 106 from manual rain gauges).

107

108 Table 1. In situ precipitation measurement networks available for Poland.

109

Observation technique	Temporal resolution	Network density / spatial resolution	Delay
Telemetric rain gauge network	10 min	1 gauge per 625 km <sup>2</sup> (about 500 gauges)	6 min (then data from more than 90% of the gauges are usually available)
Manual rain gauge network	24 hrs	1 gauge per 434 km <sup>2</sup> (about 720 gauges)	About 2 months (due to the transfer of the data and manual quality control)
Ground weather radar network	10 min	About 1 km	6 min (because the lowest scan is generated at the beginning)
Geostationary meteorological satellites (Meteosat and NWC-SAF software)	5 min (in rapid scan system)	About 5-6 km	1-5 min (due to scan strategy)

110

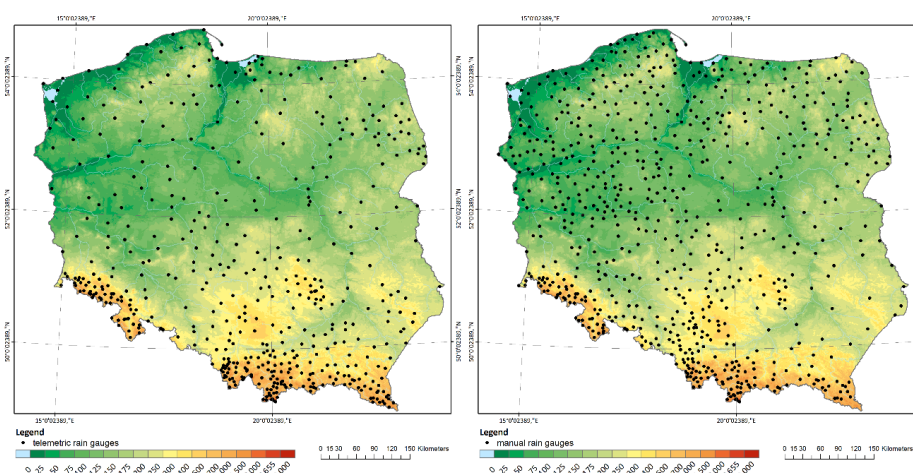


111 This study uses precipitation data generated by the Institute of Meteorology and Water  
112 Management – National Research Institute (IMGW), which performs the function of the national  
113 meteorological and hydrological service in Poland (Szturc et al., 2018). All these data are quality  
114 controlled by dedicated applications or systems.

115

## 116 2.2. Rain gauge data

117



118

119

120 **Figure 1.** Rain gauge networks of IMGW, from left: telemetric and manual rain gauge networks.

121

122 10-min precipitation accumulations are provided operationally at IMGW by a network of  
123 telemetric rain gauges, most of which are tipping-bucket gauges – considered one of the less accurate  
124 of the various types of rain gauge (Hoffmann et al., 2016; Segovia-Cardozo et al., 2021) in addition to  
125 being subject to significant failure rates. For quality control of telemetric rain gauge data, the  
126 RainGaugeQC system is used at IMGW to perform error detection and corrections on 10-min data in  
127 real-time (Ośródka et al., 2022).

128

129 One of the most important additional benefits of carrying out reanalyses, relative to the generation  
130 of a real-time precipitation field, is the possibility to exploit the much more accurate measurements  
131 performed by manual rain gauges mostly once a day. The network of such rain gauges (Hellmann type)  
132 installed at IMGW is relatively dense, and even denser than the network of telemetric rain gauges (Fig.  
133 1 and Table 1). These are the most accurate of the in situ point measurements, but they are available  
134 with a very long delay of almost two months, mainly due to the human-made data quality control. In  
135 addition, measurements from manual rain gauges are subjected to quality control in the IMGW historical  
136 database, using standard algorithms based on procedures recommended by the WMO (WMO-No. 305,  
1993, Chapter 6).



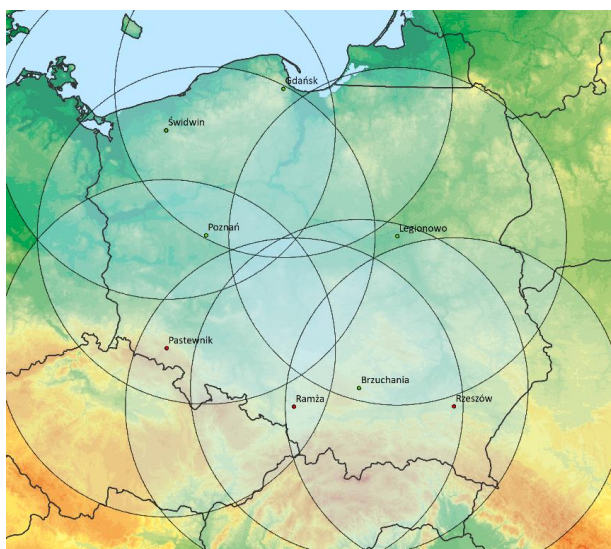
137

138 *2.3. Weather radar data*

139

140 The radar data used to generate the precipitation field estimates come from the Polish POLRAD  
141 weather radar network, operated by the IMGW. It consists of eight Doppler radars manufactured by  
142 Leonardo Germany (Fig. 2). They are currently being replaced by new models with dual-polarised radar  
143 beams, and two new radars are being installed. Three-dimensional raw data, so-called volumes (raw  
144 data), and two-dimensional products are generated by the Rainbow 5 system every 10 min (a shift to 5-  
145 min measurement frequency is currently underway), with 0.5-km spatial resolution and a range of 250  
146 km. For further details on the POLRAD network, see Ośródk and Szturc (2022).

147



148

149

150 **Figure 2.** Computational domain of Poland (900 km x 800 km) with 250-km radar coverage of the weather radar  
151 network in Poland in 2022.

152

153 The RADVOL-QC system (Ośródk et al., 2014; Ośródk and Szturc, 2022) is used to quality  
154 control of radar data of the POLRAD network, which corrects the source 3D radar data and generates  
155 dynamic maps of the data quality index. Merging data from individual radars into radar composite maps  
156 is done by applying algorithms that take account of the spatial distribution of the quality index in the  
157 radar data, which is assessed dynamically for each time step (Jurczyk et al., 2020a).

158

159 *2.4. Precipitation from meteorological satellites*

160



161 Satellite precipitation is generated by an algorithm developed at IMGW based on products  
162 provided by the EUMETSAT NWC-SAF programme (Tapiador et al., 2019). The algorithm working  
163 within RainGRS system is based on several NWC-SAF products, depicting the spatial distribution of  
164 clouds and the intensity of precipitation, including convective precipitation. A detailed description of  
165 the algorithm was presented by Jurczyk et al. (2020b).

166 Quality control of satellite precipitation is also carried out by the RainGRS system, taking into  
167 account primarily which NWC-SAF products are available at a given time. The quality of satellite  
168 precipitation, which is quantified by the quality index, is significantly lower at night-time, when visible  
169 range-based products analysing the physical properties of hydrometeors are not available.

170

### 171 **3. RainGRS system**

172

#### 173 *3.1. Merging of precipitation data into a multi-source precipitation field*

174

175 At IMGW, multi-source estimation of the precipitation field is carried out operationally by the  
176 RainGRS system. A detailed description of this system, which combines rain gauge, radar and satellite  
177 precipitation data summarised in Table 1, was presented by Jurczyk et al. (2020b). This combination  
178 algorithm takes into account the quality information of the individual input data, attributed to them when  
179 performing their quality control.

180 In operational work, the 10-min computational step of generating estimates of the precipitation  
181 field is enforced by the resolution of the radar data, which is the source of the most important high-  
182 resolution information on the spatial distribution of the precipitation field. When the radars of the  
183 POLRAD network are replaced (process in ongoing from 2022 to 2023), all included radars will operate  
184 with a 5-min time step. This will enable the temporal resolution of the multi-source precipitation  
185 estimates generated by RainGRS to be increased as well.

186 The algorithm for combining rainfall data from different sources is based on a conditional  
187 merging that attempts to enhance the strengths of the individual inputs and reduce the impact of their  
188 weaknesses. It is commonly assumed that radar data is the best representation of the spatial distribution  
189 of the precipitation field, while a network of rain gauges effectively reduces the bias of this estimation.  
190 Satellite rainfall, in contrast, plays a mainly complementary role in the absence of other data.

191 First, the rain gauge values are interpolated at radar pixel resolution, employing the Ordinary  
192 Kriging method to obtain an unbiased estimate of precipitation. The radar values at rain gauge locations  
193 and the same method of interpolation are used to get the interpolated radar field. Subsequently, the  
194 deviation between the measured and interpolated radar value ( $R - R_{int}$ ) is computed and added to the rain  
195 gauge interpolated value at each pixel of the domain, according to the following formula:

$$196 \quad R_G = G_{int} + (R - R_{int}) \quad (1)$$



197 where  $R_{int}$  is the radar precipitation interpolated from data at rain gauge locations. A satellite field  $S_G$  is  
198 obtained from an analogical formula.

199 It can be noted that the accuracy of the computed estimate depends on the distance to the nearest  
200 available rain gauge, and the radar precipitation field is preferable in the case of a long distance.  
201 Therefore, the resulting precipitation field  $R_G$  is recombined with the radar precipitation field, applying  
202 the weighted scheme, which includes the quality of individual precipitation fields to obtain a combined  
203  $GR$  field:

$$204 \quad GR = \frac{R_G \cdot QI_G + R \cdot QI_R \cdot (1 - QI_G)}{QI_G + QI_R \cdot (1 - QI_G)} \quad (2)$$

205 where  $QI_G$  and  $QI_R$  are the quality indices for gauge and radar, respectively. The quality index,  $QI$ , is  
206 the dimensionless quantity ranging from 0 (for the poorest quality) to 1 (for the best data).

207 A combined gauge-satellite field  $GS$  is obtained analogically to the above procedure, where the  
208 satellite data  $S$  and relevant quality field  $QI_S$  are taken.

209 The final quantitative precipitation estimate ( $GRS$ ) is a combination of gauge-radar and gauge-  
210 satellite fields computed by means of the following weighted formula:

$$211 \quad GRS = \frac{GR \cdot QI_d + GS \cdot (1 - QI_d) \cdot QI_S}{QI_d + QI_S \cdot (1 - QI_d)} \quad (3)$$

212 where the  $QI_d$  is a field of radar data quality as a function of the distance  $d$  to the nearest radar site.

213

### 214 3.2. Generation of daily accumulations

215

216 The basic 10-min precipitation accumulations are aggregated into different time intervals (e.g. 1-  
217 hour, several hours, daily, or longer accumulations) depending on current needs. Due to gaps in data  
218 that occur in operational work, sometimes these accumulations may not be complete. In order to ensure  
219 the completeness of the accumulations, the gaps are complemented by temporal interpolation of the data  
220 from time steps directly before and after the gap. Such averaging from neighbouring measurements is  
221 carried out if this interval is not too long, and in the opposite case data are set to have no data value. For  
222 example, when generating hourly accumulation, at most two consecutive 10-minute measurements are  
223 allowed to be missing, but no more than three terms may be missing in one hour.

224

## 225 4. Generation of daily and monthly precipitation reanalyses (RainGRS Clim)

226

### 227 4.1. Climatological reanalyses versus operational estimates

228

229 Reanalysis of the precipitation fields is carried out on daily accumulations. This provides the  
230 following benefits in terms of the reliability of the generated estimates:





- 231 1. *Complementation with data that was missing operationally due to its late arrival in the system.*  
232 For reanalyses, a time regime is not as strict as in an operational work, so data that arrived too  
233 late can be included. In the operational RainGRS, more than 90% of the rain gauge data  
234 generally arrives within six minutes, so the remaining data can be involved in reanalyses.  
235 When it comes to radar data, delays mainly affect data from foreign radars.
- 236 2. *The use of measurement techniques that are available too late to be used operationally, or that*  
237 *take measurements with a time step longer than 10 minutes as standard.* In the proposed  
238 algorithm for performing reanalyses, in addition to using daily precipitation accumulations  
239 provided by those measurement techniques from which data are operationally available, data  
240 from manual rain gauges can also be used. These measurements are taken only once a day and  
241 are available after about two months – for this reason they are not used in the operational  
242 version of RainGRS, but due to their high reliability these data are very important, even  
243 crucial.
- 244 3. *Greater effectiveness of quality control and data merging algorithms when applied to*  
245 *accumulations longer than 10 minutes, e.g. daily.* Longer precipitation accumulations are more  
246 consistent, as they are much less affected by temporal inconsistencies between different  
247 measurement techniques (this is especially the case with radar measurements, which in  
248 practice are instantaneous), and are moreover less sensitive to errors of a random nature, which  
249 become more averaged over a longer time interval. Thus, the algorithms for both quality  
250 control and multi-source combination perform more effectively.

251 At IMGW, combined daily accumulations have been generated since 2021 by the algorithm  
252 described in this paper. The resulting daily precipitation estimates can already be directly used to  
253 generate longer precipitation accumulations, e.g. monthly, seasonal, annual or even multi-year. In view  
254 of the above possibilities, which create new areas of application for multi-source precipitation fields,  
255 e.g. in climatology, the version of RainGRS that generates reanalyses of daily precipitation accumulation  
256 is referred to as the climatology version RainGRS Clim.

257

#### 258 4.2. *Algorithm for the estimation of climatological multi-source precipitation fields*

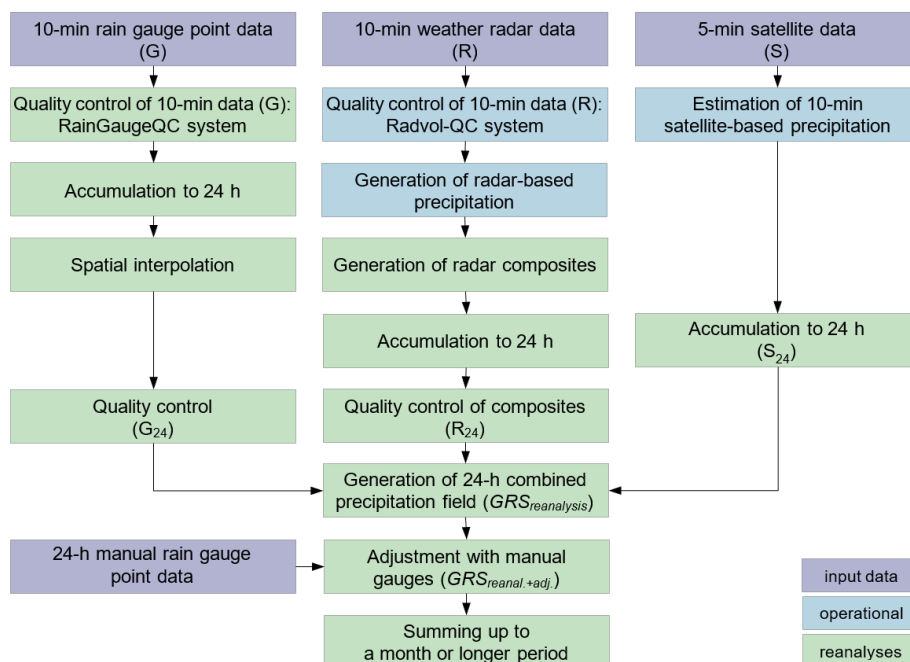
259

260 The algorithm presented in this section for calculating quality-controlled daily and monthly  
261 rainfall totals follows the following scheme (Fig. 3):

- 262 1. Daily totals are calculated from 10-min rain gauge data. In order to ensure the completeness  
263 of the 10-min data, missing rain gauge data is completed with spatially interpolated values  
264 from the data that are available. The Ordinary Kriging method is used to interpolate the data.
- 265 2. The daily point accumulations from the rain gauges are spatially interpolated to obtain  
266 precipitation fields.



- 267 3. A human expert check of the daily rain gauge fields is carried out, during which erroneous  
268 values from individual rain gauges are removed. This check on the daily values enables the  
269 detection of errors that were not detected on the 10-min accumulations with automatic QC  
270 algorithms. The daily accumulations from the rain gauges are then spatially interpolated again  
271 (as in point 2).
- 272 4. Daily accumulations of radar and satellite precipitation fields are calculated, also  
273 supplemented with late data.
- 274 5. The daily radar precipitation fields are corrected by removing disturbances occurring at the  
275 locations of some radars, as this correction only works effectively on longer accumulations.
- 276 6. Estimates of daily accumulations  $GRS_{reanalysis}$  are calculated by the RainGRS system using  
277 the algorithm described in Section 3.1, which uses daily accumulations of individual  
278 precipitation fields as input data. This approach minimises errors associated with temporal  
279 inconsistencies in the data (Villalobos-Herrera et al., 2022).
- 280 7. An adjustment of daily accumulations calculated by the RainGRS to observations from manual  
281 rain gauges, which are considered the most reliable point estimate of rainfall, is performed.  
282 The adjustment factor is determined separately for each manual rain gauge location and then  
283 spatially interpolated using the inverse distance weighting method to distribute it spatially  
284 (Wang et al., 2020). This adjustment results in daily accumulations  $GRS_{reanal.+adj.}$  of multi-  
285 source rainfall fields after reanalysis and adjustment.
- 286 8. The long-term accumulations of the combined precipitation fields (e.g., monthly) can be  
287 calculated from the daily accumulations prepared in the above manner.  
288



289

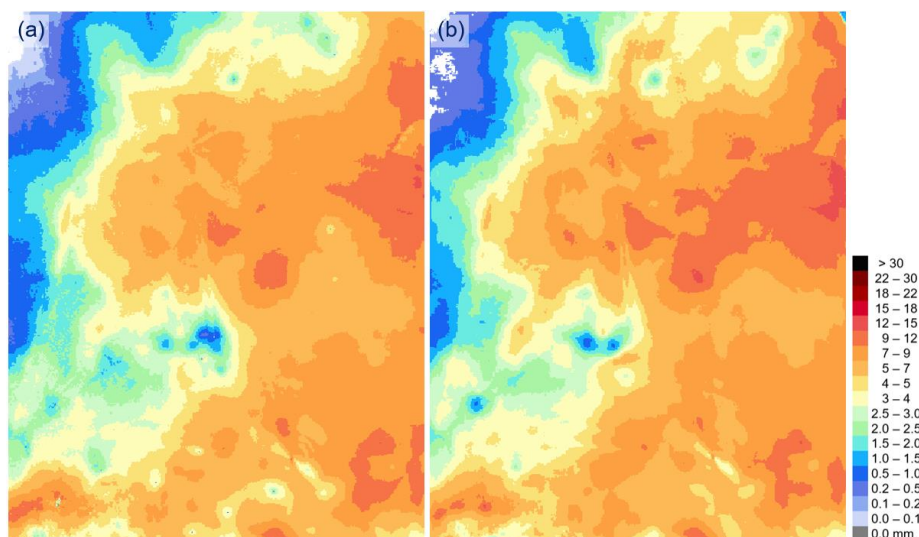
290

291 **Figure 3.** The algorithm for determining quality-controlled daily, monthly, and other precipitation accumulations.

292

293 Fig. 4 shows an example of daily rainfall accumulations obtained operationally and after  
 294 reanalysis. The differences between the two fields are generally not large, but locally they can be quite  
 295 significant – a fragment from the computational domain is selected to highlight them. Larger differences  
 296 between them are apparent in cases where some rain gauge data have been removed as a result of manual  
 297 QC (during which they were found to be clearly erroneous) and which was not recognised by operational  
 298 control. It is likely that in the 10-min accumulations the measurement errors were not so noticeable as  
 299 to consider these values to be completely erroneous. The removal of each such value also affects the  
 300 values in a certain vicinity of the rain gauge’s location due to changes in the field of interpolated gauges,  
 301 relevant QI field and consequently in the RainGRS field. In addition, some of the differences between  
 302 the two fields are due to the varying performance of the data combination algorithm (Sect. 3.1) on daily  
 303 accumulations when compared to 10-min ones.

304



305

306

307 **Figure 4.** Fields of daily precipitation accumulations, before and after reanalysis: (a)  $GRS_{real-time}$  and (b)  
308  $GRS_{reanalysis}$ . Fragment of Poland’s computational domain (325 km x 425 km), 11 December 2022.

309

## 310 5. Verification

311

### 312 5.1. Methodology of the verification

313

314 In order to verify any precipitation field estimate, a precipitation field reference that can be  
315 considered as a “ground truth” is needed. Lysimeters are regarded as one of the most accurate point  
316 precipitation measurement techniques, but Hellmann-type manual rain gauges have similar reliability  
317 (Hoffmann et al., 2016). IMGW does not have at its disposal a network of lysimeters, however, it does  
318 have a relatively dense network of manual Hellmann type rain gauges, therefore these were considered  
319 to provide the most accurate technique of point measurement of precipitation available in IMGW. Thus,  
320 the results obtained in the present study were verified on them.

321

322 However, it should be borne in mind that the data from the manual rain gauges are not  
323 independent, as they have previously been used for adjustment of the RainGRS Clim data. Thus, the  
324 basic quantity verified in this Section is not the final precipitation estimates produced after adjustment  
325 to the manual rain gauge data, but the estimates after quality control and reanalysis, i.e.,  $GRS_{reanalysis}$ .  
326 However, the verification of the final reanalyses  $GRS_{reanal.+adj.}$  also provides interesting information,  
327 though one should be careful especially with criteria directly related to the estimated values, such as  
BIAS or RMSE, rather than, for example, their correlation with the reference field.



328 The period from January 2021 to December 2022 was analysed. For each of these 24 months, the  
329 statistics of the monthly precipitation estimates BIAS, RRSE, RMSE, and CC were calculated, taking  
330 the accumulations from the manual rain gauges as reference:

331

332 – statistical bias:

$$333 \quad \text{BIAS} = \frac{1}{n} \sum_{i=1}^n (F_i - O_i) \quad (4)$$

334 – root mean square error:

$$335 \quad \text{RMSE} = \sqrt{\frac{1}{n} \sum_{i=1}^n (F_i - O_i)^2} \quad (5)$$

336 – root relative square error:

$$337 \quad \text{RRSE} = \frac{\sqrt{\sum_{i=1}^n (F_i - O_i)^2}}{\sqrt{\sum_{i=1}^n (O_i - \bar{O})^2}} \quad (6)$$

338 – Pearson correlation coefficient:

$$339 \quad \text{CC} = \frac{\sum_{i=1}^n (F_i - \bar{F})(O_i - \bar{O})}{\sqrt{\sum_{i=1}^n (O_i - \bar{O})^2 \sum_{i=1}^n (F_i - \bar{F})^2}} \quad (7)$$

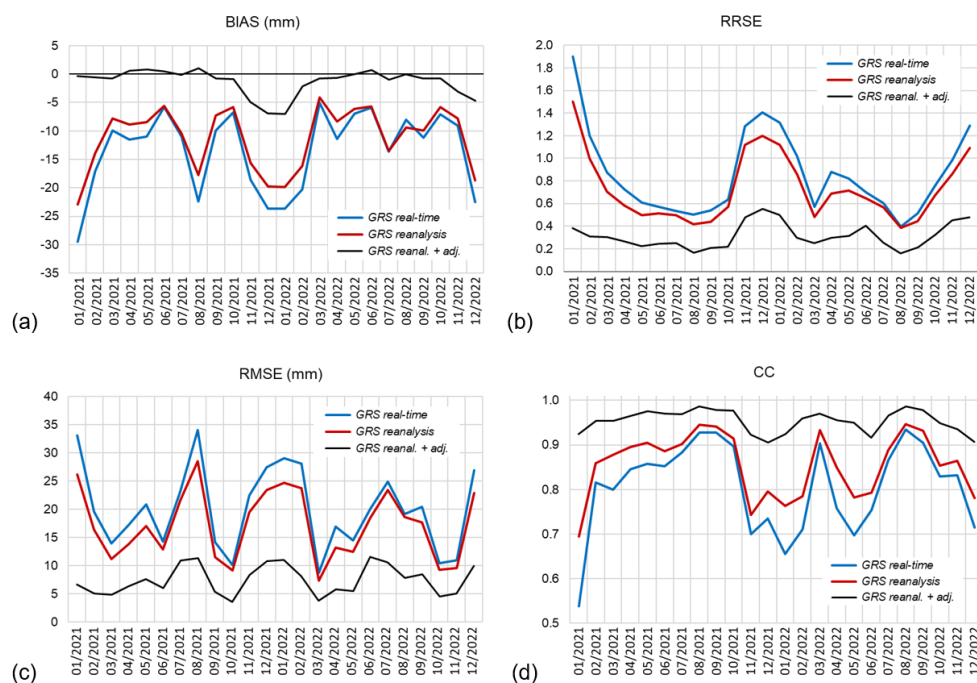
340

341 where  $F_i$  is the assessed value,  $O_i$  is the reference value (from manual rain gauges),  $i$  is the pixel number,  
342  $n$  is the number of pixels, a  $\bar{F}$  and  $\bar{O}$  are the mean values of  $F_i$  and  $O_i$ .

343

344 *5.2. Monthly statistics*

345



346  
347

**Figure 5.** Values of monthly characteristics: (a) BIAS, (b) RRSE, (c) RMSE, (d) CC, for precipitation estimates  $GRS_{real-time}$ ,  $GRS_{reanalysis}$ , and  $GRS_{reanal.+adj.}$  for consecutive months, using point data from manual rain gauges as reference. Data for 2021 and 2022.

350  
351

Figure 5 shows how the values of the four statistics BIAS, RRSE, RMSE, and CC, change in the following months, i.e. depending on the seasonal precipitation characteristics.

354

The most evident phenomenon visible in the BIAS graph is large underestimation of monthly precipitation accumulations, especially in winter months (December – February) that can reach up to 20 mm (Fig. 5a), which in Poland means several dozen percent of monthly accumulations. This is a result of the fact that the precipitation measurements from both rain gauges and radars are underestimated in IMGW due to the use of specific types of measuring devices, as mentioned in Sections 2.2 and 2.3. Additionally, in winter the reason for these errors is the difficulty in radar measurements that occurs during snowfall from lower clouds than in other seasons and causes most of this precipitation to become invisible to radar as a result of overshooting the precipitation by the radar beam.

362

Reanalysis and quality control on daily accumulations leads to a reduction of BIAS by a few mm per month, mainly in the winter months. This is mostly due to the clearly better performance of the algorithm for the combination of rain gauge and radar data, which copes better with low precipitation on longer accumulations. After adjustment to observations from manual rain gauges it is possible to deal with the problem of underestimation of the precipitation field – the BIAS is then practically eliminated,

366



367 and is visible only to a small extent, mainly in winter. But even then, it is reduced several times, to  
368 approximately -7 mm per month (Fig. 5a). In warmer seasons the observed BIAS values are relatively  
369 smaller, though August 2021 is a clear outlier. Such large errors in this month, visible not only in BIAS  
370 but also in RMSE, are due to the fact that this month was characterised by extremely high precipitation:  
371 the monthly total for a large part of southern Poland was over 300 mm, while in this region the multi-  
372 year average precipitation in August is about 100 mm. High precipitation accumulations are  
373 automatically associated with an increase in the values of statistics of an absolute nature, so that they  
374 are not visible in the values of relative statistics such as RRSE and CC.

375 The RRSE annual cycle (Fig. 5b) also shows the largest estimation errors in winter. The error is  
376 rather high in winter, at about 1.3 – 1.4 for  $GRS_{real-time}$ , and the reanalysis improved the reliability of  
377 the precipitation estimate, resulting in a decrease of the RRSE to a value of about 1.1 – 1.2. For the other  
378 months, the error is lower, at about 0.5 for  $GRS_{real-time}$ , and the reanalysis improved the reliability of  
379 the estimate to a lesser extent, as the RRSE decreased by about 0.1.

380 High values of RMSE (Fig. 5c) are observed in winter, when they reach 27-29 mm for  
381  $GRS_{real-time}$ , but unlike RRSE, they also occur in the summer months, which is related to the frequent  
382 occurrence of intense convective precipitation during this season. They do not induce a similar increase  
383 in RRSE values, because this statistic is relative as the result of dividing the RMSE by the standard  
384 deviation from the reference value (Eq. 6). Reanalysis reduces RMSE values in winter by about 5 mm  
385 per month, slightly less in the other seasons, and adjustment to manual rain gauges reduces them to  
386 values of about 5-10 mm per month independently of the season.

387 The correlation coefficient CC (Fig. 5d) is more sensitive to the existence of relationship between  
388 evaluated and reference data than the other statistics, which are based on the comparison of estimated  
389 and reference values. The CC values also indicate the lowest reliability of the precipitation estimates in  
390 winter, when the coefficient equals about 0.65 and improves to about 0.75 after reanalysis. The reason  
391 for these low values can also be explained by the low variability of the precipitation accumulations over  
392 this period, which results in a low correlation with the manual rain gauge measurements. In other  
393 seasons, especially in the summer months, the CC values are much higher, as they reach approximately  
394 0.8 – 0.9 for both operational and reanalysed estimates. The adjustment to the manual rain gauges  
395 increases the correlations to approximately 0.9 – 0.95.

396 In March 2022, there was a noticeable deviation from the typical annual pattern described above  
397 for the CC coefficient. This was due to the exceptionally dry period that occurred at that time in the  
398 whole country, particularly in northern Poland. Typically, monthly precipitation accumulation for  
399 March is around 30-40 mm in Poland, but in 2022 it was significantly lower, and in the northern part of  
400 the country it was often even zero. In this case, the correlation coefficient usually increases, so that in  
401 this particular month, the correlation value for  $GRS_{real-time}$  was as high as 0.90, rising to 0.93 after  
402 reanalysis. Another unexpected value of the CC coefficient was observed in May 2022, when the  
403 correlation is around 0.7, which was improved by reanalysis and adjustment, after which the CC



404 increased to around 0.95. The reason for this effect was probably a Legionowo radar replacement at that  
 405 time, because this radar covers a large part of the domain where other radars do not reach.

406 In general, the reliability of monthly estimates of precipitation field accumulation is clearly  
 407 dependent on the season. Two evident phenomena can be observed here: in winter (November –  
 408 February), high values of BIAS, RRSE, and RMSE are noticeable at the same time as low values of CC,  
 409 as indicated in the above analysis. In summer (July – August), the situation is different, as convective,  
 410 thunderstorm precipitation is often observed during this time, so the intensity of precipitation is higher,  
 411 and monthly accumulations are much higher, which is also reflected in the RMSE values, while the  
 412 correlation (CC) with the reference data is then significantly higher.

413 Table 2 summarises statistics for two selected months from 2022: January for winter and August  
 414 for summer. The table shows the values of quality metrics for the three multi-source precipitation fields:  
 415 operationally generated ( $GRS_{real-time}$ ), after reanalysis ( $GRS_{reanalysis}$ ), and after adjustment of this  
 416 reanalysed precipitation field ( $GRS_{reanal.+adj.}$ ), with manual rain gauge observations as a reference. All  
 417 statistics are worse for winter than for summer, however, reanalysis as well as adjustment worked much  
 418 more effectively in winter. Precipitation reanalysis, involving merging individual rainfall fields on daily  
 419 (instead of 10-min) accumulations, along with the associated more effective data quality control, results  
 420 in a clear improvement in all quality statistics in winter (January 2022), e.g. RMSE by almost 4.5 mm  
 421 and CC by 0.1. In summer (August 2022), however, this impact is much smaller, and amounts to less  
 422 than 0.6 mm and 0.02, respectively, but BIAS slightly increased. The further improvement, which results  
 423 from adjustment to data from manual rain gauges, is much more evident – in winter it is more than 13.5  
 424 mm in RMSE and 0.16 in CC, and in summer more than 11.8 mm and 0.04, respectively.

425  
 426 Table 2. Values of quality metrics for merged daily precipitation fields: before reanalysis ( $GRS_{real-time}$ ), after  
 427 reanalysis ( $GRS_{reanalysis}$ ), and after reanalysis and adjustment ( $GRS_{reanal.+adj.}$ ), using point data from manual  
 428 rain gauges as reference. Months: (a) January 2022, (b) August 2022.

429

430 (a) January 2022

Metric	BIAS (mm)	RMSE (mm)	RRSE (--)	CC (--)
$GRS_{real-time}$	-23.72	29.04	1.32	0.66
$GRS_{reanalysis}$	-19.83	24.63	1.12	0.76
$GRS_{reanal.+adj.}$	-7.06	11.06	0.50	0.92

431

432 (b) August 2022

Metric	BIAS (mm)	RMSE (mm)	RRSE (--)	CC (--)
$GRS_{real-time}$	-8.04	19.18	0.40	0.93
$GRS_{reanalysis}$	-9.35	18.60	0.38	0.95





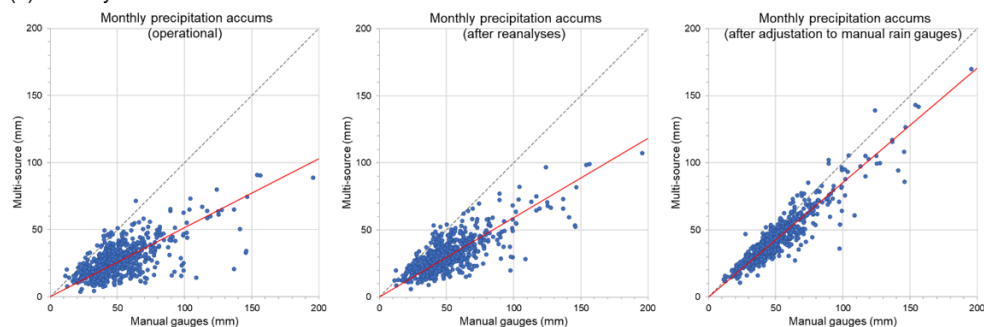
$GRS_{reanal.+adj.}$	-0.03	7.77	0.16	0.99
----------------------	-------	------	------	------

433

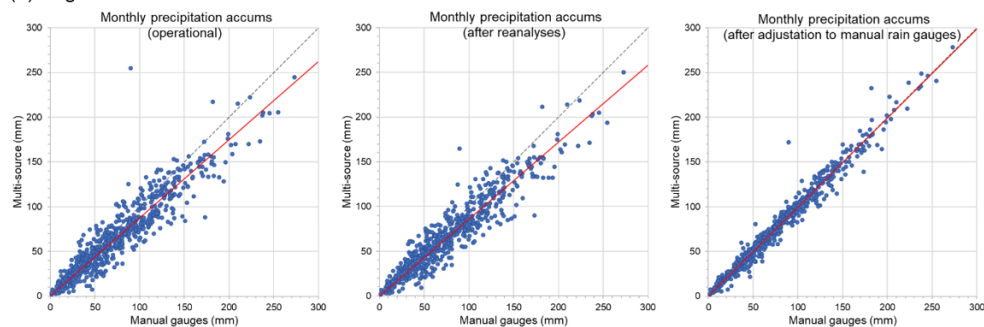
434 Concluding, for all the statistics used here, the improvement in the quality of monthly  
 435 accumulation of estimated precipitation fields  $GRS_{reanalysis}$  i  $GRS_{reanal.+adj.}$  relative to operational  
 436 fields  $GRS_{real-time}$  is clearly visible. The differences between the statistics of  $GRS_{reanal.+adj.}$  and  
 437  $GRS_{real-time}$  are much larger. This is mainly due to the fact that, in the absence of any other possibility,  
 438 the verification was carried out using data from manual rain gauges as a reference, and here they are  
 439 dependent data, as they are used during the generation of the final  $GRS_{reanal.+adj.}$  (see point 7 in the  
 440 data processing scheme in Section 4.2).

441

(a) January 2022



(b) August 2022



442

443

444 **Figure 6.** Plots of the dependence of monthly precipitation estimate values, from left:  $GRS_{real-time}$ ,  $GRS_{reanalysis}$   
 445 and  $GRS_{reanal.+adj.}$  on values measured with manual rain gauges, along with trend lines. Months: (a) January  
 446 2022, (b) August 2022.

447

448 Fig. 6 shows graphs of the relationship between the estimated fields of monthly accumulated  
 449 RainGRS precipitation calculated operationally (generated in real-time), after reanalysis and after  
 450 adjustment of this reanalysed precipitation field, and monthly accumulations observed by manual rain

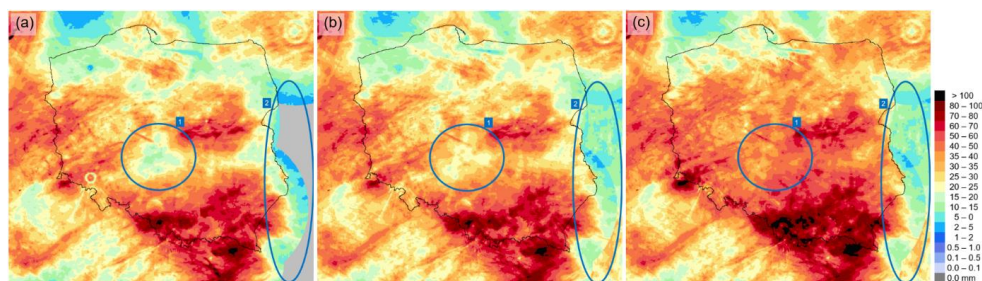


451 gauges, for the same two months for which the values of statistics are summarised in Table 2. The graphs  
452 show precipitation values at locations of manual rain gauges. The correlation for the  $GRS_{reanalysis}$   
453 estimate compared to  $GRS_{real-time}$  improved, although only slightly. This conformity, measured by the  
454 distance between the trend line (red) and the one-to-one line (dashed), clearly improved in winter, but  
455 declined slightly in summer. The conformity with manual rain gauges for the  $GRS_{reanal.+adj.}$  estimate  
456 is clearly greater than that for the  $GRS_{reanalysis}$ , but it should be borne in mind that the data from manual  
457 rain gauges are not fully independent. Nevertheless, this comparison gives some information about the  
458 effectiveness of the final step in generating precipitation field estimates with the RainGRS Clim system.

459

## 460 6. Example of a climatological estimate of monthly precipitation accumulation

461



462

463

464 **Figure 7.** Fields of monthly precipitation accumulations: (a)  $GRS_{real-time}$ , (b)  $GRS_{reanalysis}$ , and (c)  
465  $GRS_{reanal.+adj.}$ . Domain of Poland, April 2021.

466

467 In Fig. 7 we can see an example of estimates of monthly precipitation accumulations for the  
468 domain of Poland, 900 km x 800 km (see Fig. 2). From the left there are estimates: operational, after the  
469 reanalysis, and after reanalysis and adjustment to manual rain gauges data. In general, values of the  
470 estimated precipitation increased after the reanalysis as a result of the more effective performance of the  
471 merging algorithm on longer accumulations. After the adjustment to manual rain gauges, the further,  
472 much higher increase of the precipitation values is because radar-based precipitation estimates are  
473 underestimated in the case of Polish weather radars. Moreover, it should be taken into account that rain  
474 gauges also underestimate rainfall, because they are mostly tipping bucket devices (Segovia-Cardozo et  
475 al., 2021).

476 The area of underestimated precipitation in the centre of Poland marked with “1” in Fig. 7 is the  
477 place where the distance to the closest radar site is longest – more than 200 km, where the radar beam  
478 passes over part of the precipitation (overshoots). Moreover, the telemetric rain gauge network is rather  
479 sparse here. Adjustment to manual rain gauges has made it possible to correct this underestimation.

480 The area denoted “2” in Fig. 7 indicates the region where there are no radars, even from  
481 neighbouring countries. Reanalysis partially improves it by complementing the lack of data with



482 satellite-based precipitation, but not wholly effectively due to the higher uncertainty of the satellite  
483 estimates.

484

## 485 7. Conclusions

486

487 The following general conclusions can be drawn about the proposed methodology for the  
488 generation of long-term precipitation estimates by the RainGRS Clim system:

- 489 1. Based on an analysis of available precipitation data, it was assumed that the most reliable  
490 precipitation measurement technique is a network of manual rain gauges. In particular, it was  
491 assumed that these measurements are unbiased. Since their daily accumulations are available  
492 with a long delay due to their transfer and manual quality control, they cannot be used in real  
493 time, but they can be used effectively to perform adjustment of reanalyses (see Sections 5.2  
494 and 5.3).
- 495 2. The second major limitation of manual rain gauges is that they only provide point observations.  
496 However, the relatively high density of this measurement network in Poland (Fig. 1) makes  
497 them very useful in the adjustment of other precipitation field estimates.
- 498 3. With daily accumulations, which, due to the time step of manual rain gauge measurements,  
499 are the basic accumulations in the algorithm for generating climatological precipitation  
500 estimates described in Section 4.2, it becomes possible to perform much more effective quality  
501 control, particularly in terms of removing various types of artifacts in weather radar data.
- 502 4. Algorithms for merging rain gauge, weather radar, and satellite data perform much more  
503 effectively for daily totals than for 10-min totals. This is mainly due to the fact that longer  
504 accumulations of precipitation are more consistent, as in this case time inconsistencies  
505 between different measurement techniques play a much smaller role. In addition, with longer  
506 accumulations, errors of a random nature are more averaged out (see Section 4.1).
- 507 5. The results presented in the paper show that after reanalysis, estimates of precipitation field  
508 are of higher reliability than operationally generated estimates. Adjustment of the data after  
509 reanalysis to data from manual rain gauges resulted in a further, much higher quality  
510 improvement (Sections 5.2 and 5.3). However, it should be kept in mind that the final estimates  
511 are obtained using data from manual rain gauges, so the results of the verification performed  
512 on these data, which in this case are partially dependent, should be treated with caution.
- 513 6. Having estimates of precipitation accumulated over longer time intervals in RainGRS Clim,  
514 such as monthly intervals, creates the possibility of applying them to climatological analyses.  
515 They provide valuable information, especially when high spatial resolution of precipitation  
516 data is important.

517



518 *Code availability.* The data processing codes are protected through the economic property rights to the software  
519 and are not available for distribution. The codes used for processing follow the methodologies and equations  
520 described herein.

521

522 *Data availability.* The data used in this paper are available upon request.

523

524 *Author contributions.* AJ, KO, JS, and MP designed algorithms of the RainGRS Clim system. MP, KO, and AK  
525 developed the software code and performed the simulations. JS, KO, AJ, AK, and MP prepared the paper. JS made  
526 figures.

527

528 *Competing interests.* The contact author has declared that none of the authors has any competing interests.

529

## 530 **References**

531

532 Bonaccorso, B., Brigandì, G., Aronica, G. T., 2020. Regional sub-hourly extreme rainfall estimates in  
533 Sicily under a scale invariance framework, *Water Resources Management*, **34**, 4363-4380,  
534 <https://doi.org/10.1007/s11269-020-02667-5>.

535 Burcea, S., Cică, R., Bojariu, R., 2019. Radar-derived convective storms' climatology for the Prut River  
536 basin: 2003–2017, *Natural Hazards and Earth System Sciences*, **19**, 1305-1318,  
537 <https://doi.org/10.5194/nhess-19-1305-2019>.

538 Chan, S. C., Kendon, E. J., Roberts, N. M., Fowler, H. J., Blenkinsop, S., 2016. The characteristics of  
539 summer sub-hourly rainfall over the southern UK in a high-resolution convective permitting  
540 model. *Environmental Research Letters*, **11**, 094024, [https://doi.org/10.1088/1748-](https://doi.org/10.1088/1748-9326/11/9/094024)  
541 [9326/11/9/094024](https://doi.org/10.1088/1748-9326/11/9/094024).

542 Fabry, F., Meunier, V., Treserras, B. P., Courmoyer, A., and Nelson, B., 2017. On the Climatological  
543 Use of Radar Data Mosaics: Possibilities and Challenges, *Bulletin of the American*  
544 *Meteorological Society*, **98**, 2135-2148, <https://doi.org/10.1175/BAMS-D-15-00256.1>.

545 Hamidi, A., Devineni, N., Booth, J. F., Hosten, A., Ferraro, R. R., Khanbilvardi, R., 2017. Classifying  
546 urban rainfall extremes using weather radar data: An application to the greater New York area,  
547 *Journal of Hydrometeorology*, **18**, 611-623, <https://doi.org/10.1175/JHM-D-16-0193.1>.

548 Hänsler, A., Weiler, M., 2022. Enhancing the usability of weather radar data for the statistical analysis  
549 of extreme precipitation events, *Hydrology and Earth System Sciences*, **26**, 5069–5084,  
550 <https://doi.org/10.5194/hess-26-5069-2022>.

551 Hoffmann, M., Schwartengraber, R., Wessolek, W., Peters, A., 2016. Comparison of simple rain gauge  
552 measurements with precision lysimeter data, *Atmospheric Research*, **174-175**, 120-123,  
553 <https://doi.org/10.1016/j.atmosres.2016.01.016>.



- 554 Imhoff, R., Brauer, C., van Heeringen, K.-J., Leijnse, H., Overeem, A., Weerts, A., Uijlenhoet, R., 2021.  
555 A climatological benchmark for operational radar rainfall bias reduction, *Hydrology and Earth*  
556 *System Sciences*, **25**, 4061–4080, <https://doi.org/10.5194/hess-25-4061-2021>, 2021.
- 557 Jurczyk, A., Szturc, J., Ośródką, K., 2020a. Quality-based compositing of weather radar QPE estimates,  
558 *Meteorological Applications*, **27**, e1812, <https://doi.org/10.1002/met.1812>.
- 559 Jurczyk, A., Szturc, J., Otop, I., Ośródką, K., Struzik, P., 2020b. Quality-based combination of multi-  
560 source precipitation data. *Remote Sensing*, **12**, 1709, <https://doi.org/10.3390/rs12111709>.
- 561 Klok, E. J., Klein Tank, A. M. G., 2009. Updated and extended European dataset of daily climate  
562 observation, *International Journal of Climatology*, **29**, 1182–1191,  
563 <https://doi.org/10.1002/joc.1779>, 2008.
- 564 Lengfeld, K., Kirstetter, P.-E., Fowler, H. J., Yu, J., Becker, B., Flamig, Z., Gourley, J., 2020. Use of  
565 radar data for characterizing extreme precipitation at fine scales and short durations,  
566 *Environmental Research Letters*, **15**, 085003, <https://doi.org/10.1088/1748-9326/ab98b4>.
- 567 Marra, F., Armon, M., Morin, E., 2022. Coastal and orographic effects on extreme precipitation revealed  
568 by weather radar observations, *Hydrology and Earth System Sciences*, **26**, 1439–1458,  
569 <https://doi.org/10.5194/hess-26-1439-2022>.
- 570 Morbidelli, R., Saltalippi, C., Flammini, A., Corradini, C., Wilkinson, S. M., Fowler, H. J., 2018.  
571 Influence of temporal data aggregation on trend estimation for intense rainfall, *Advances in Water*  
572 *Resources*, **122**, 304–316, <https://doi.org/10.1016/j.advwatres.2018.10.027>.
- 573 Neuper, M., Ehret, U., 2019. Quantitative precipitation estimation with weather radar using a data- and  
574 information-based approach. *Hydrology and Earth System Sciences*, **23**, 3711–3733,  
575 <https://doi.org/10.5194/hess-23-3711-2019>.
- 576 Ochoa-Rodriguez, S., Wang, L.-P., Willems, P., Onof, C., 2019. A review of radar-rain gauge data  
577 merging methods and their potential for urban hydrological applications. *Water Resources*  
578 *Research*, **55**, 6356–6391. <https://doi.org/10.1029/2018WR023332>.
- 579 Ośródką K., Szturc J., Jurczyk A., 2014. Chain of data quality algorithms for 3-D single-polarization  
580 radar reflectivity (RADVOL-QC system). *Meteorological Applications*, **21**, 256–270,  
581 <https://doi.org/10.1002/met.1323>.
- 582 Ośródką, K., Szturc, J., 2022. Improvement in algorithms for quality control of weather radar data  
583 (RADVOL-QC system), *Atmospheric Measurement Techniques*, **15**, 261–277,  
584 <https://doi.org/10.5194/amt-15-261-2022>.
- 585 Ośródką, K., Otop, I., Szturc, J., 2022. Automatic quality control of telemetric rain gauge data providing  
586 quantitative quality information (RainGaugeQC), *Atmospheric Measurement Techniques*, **15**,  
587 5581–5597, <https://doi.org/10.5194/amt-15-5581-2022>.
- 588 Overeem, A., van den Besselaar, E., van der Schrier, G., Meirink, J. F., van der Plas, E., Leijnse, H.,  
589 2023. EURADCLIM: the European climatological high-resolution gauge-adjusted radar



- 590 precipitation dataset, *Earth System Science Data*, **15**, 1441–1464, [https://doi.org/10.5194/essd-](https://doi.org/10.5194/essd-15-1441-2023)  
591 15-1441-2023.
- 592 Park, S., Berenguer, M., Sempere-Torres, D., 2019. Long-term analysis of gauge-adjusted radar rainfall  
593 accumulations at European scale, *Journal of Hydrology*, **573**, 768–777,  
594 <https://doi.org/10.1016/j.jhydrol.2019.03.093>.
- 595 Piscitelli, F.M., Ruiz, J.J., Negri, P., Salio, P., 2022. A multiyear radar-based climatology of supercell  
596 thunderstorms in central-eastern Argentina, *Atmospheric Research*, **277**, 106283,  
597 <https://doi.org/10.1016/j.atmosres.2022.106283>.
- 598 Saltikoff, E., Friedrich, K., Soderholm, J., Lengfeld, K., Nelson, B., Becker, A., Hollmann, R., Urban,  
599 B., Heistermann, M., Tassone, C., 2019a. An overview of using weather radar for climatological  
600 studies: Successes, challenges, and potential, *Bulletin of the American Meteorological Society*,  
601 **100**, 1739–1752, <https://doi.org/10.1175/BAMS-D-18-0166.1>.
- 602 Saltikoff, E., Haase, G., Delobbe, L., Gaussiat, N., Martet, M., Idziorek, D., Leijnse, H., Novák, P.,  
603 Lukach, M., Stephan, K., 2019b. OPERA the radar project, *Atmosphere*, **10**, 320,  
604 <https://doi.org/10.3390/atmos10060320>.
- 605 Segovia-Cardozo, D.A., Rodríguez-Sinobas, L., Díez-Herrero, A., Zubelzu, S., Canales-Ide, F.,  
606 2021. Understanding the mechanical biases of tipping-bucket rain gauges: A semi-  
607 analytical calibration approach. *Water*, **13**, 2285, <https://doi.org/10.3390/w13162285>.
- 608 Sokol, Z., Szturc, J., Orellana-Alvear, J., Popová, J., Jurczyk, A., Célleri, R., 2021. The role of weather  
609 radar in rainfall estimation and its application in meteorological and hydrological modelling – A  
610 review. *Remote Sensing*, **13**, 351, <https://doi.org/10.3390/rs13030351>.
- 611 Szturc, J., Jurczyk, A., Ośródk, K., Wyszogrodzki, A., Giszterowicz, M., 2018. Precipitation estimation  
612 and nowcasting at IMGW-PIB (SEiNO system), *Meteorology Hydrology and Water  
613 Management*, **6**, 3–12, <https://doi.org/10.26491/mhwm/76120>.
- 614 Tapiador, F.J.; Marcos, C.; Sancho, J.M. The convective rainfall rate from cloud physical properties  
615 algorithm for Metaset Second-Generation satellites: Microphysical basis and intercomparisons  
616 using an object-based method. *Remote Sensing*, 2019, **11**, 527,  
617 <https://doi.org/10.3390/rs11050527>.
- 618 Villalobos-Herrera, R., Blenkinsop, S., Guerreiro, S.B., O’Hara, T., Fowler, H.J., 2022. Sub-hourly  
619 resolution quality control of rain gauge data significantly improves regional sub-daily return level  
620 estimates, *Quarterly Journal of the Royal Meteorological Society*, **148**, 3252–3271,  
621 <https://doi.org/10.1002/qj.4357>.
- 622 Voormansik, T., Mürsepp, T., Post, P. 2021. Climatology of Convective Storms in Estonia from Radar  
623 Data and Severe Convective Environments. *Remote Sensing*, **13**, 2178. [https://](https://doi.org/10.3390/rs13112178)  
624 [doi.org/10.3390/rs13112178](https://doi.org/10.3390/rs13112178).



- 625 Wagner, A., Seltmann, J., Kunstmann, H., 2012. Joint statistical correction of clutters, spokes and beam  
626 height for a radar derived precipitation climatology in southern Germany, *Hydrology and Earth*  
627 *System Sciences*, **16**, 4101–4117, <https://doi.org/10.5194/hess-16-4101-2012>.
- 628 Wang, K.-H., Chu, T., Yang, M.-D., Chen, M.-C., 2020. Geostatistical based models for the spatial  
629 adjustment of radar rainfall data in typhoon events at a high-elevation river watershed. *Remote*  
630 *Sensing*, **12**, 1427. <https://doi.org/10.3390/rs12091427>.
- 631 Wetchayont, P., Ekkawatpanit, C., Rueangrit, S., Manduang, J., 2023. Improvements in rainfall  
632 estimation over Bangkok, Thailand by merging satellite, radar, and gauge rainfall datasets with  
633 the geostatistical method, *Big Earth Data*, <https://doi.org/10.1080/20964471.2023.2171581>.  
634 (Early View).
- 635 WMO-No. 305, 1993. *Guide on the Global Data-processing System*, World Meteorological  
636 Organization, Geneva, 199 pp., ISBN 978-92-63-13305-2,  
637 [https://library.wmo.int/index.php?lvl=notice\\_display&id=6832#.Y1AI4uTP2Uk](https://library.wmo.int/index.php?lvl=notice_display&id=6832#.Y1AI4uTP2Uk).  
638